PCCP

Accepted Manuscript

ROYAL SOCIETY OF CHEMISTRY

www.rsc.org/pccp

Journal Name

RSCPublishing

ARTICLE

The Fate of Phenothiazine-Based Redox Shuttles in Lithium-Ion Batteries

Cite this: DOI: 10.1039/xoxxoooooox

Matthew D. Casselman,[1] Aman Preet Kaur,[1] Kishore Anand Narayana,[1] Corrine F. Elliott,[1] Chad Risko,[1,2]* and Susan A. Odom[1]*

Received ooth January 2012,
Accepted ooth January 2012

DOI: 10.1039/xoxxoooooox

www.rsc.org/

The stability and reactivity of the multiple oxidation states of aromatic compounds are critical to the performance of these species as additives and electrolytes in energy-storage applications. Both for the overcharge mitigation in ion-intercalation batteries and as electroactive species in redox flow batteries, neutral, radical-cation, and radical-anion species may be present during charging and discharging processes. Despite the wide range of compounds evaluated for both applications, the progress identifying stable materials has been slow, imited perhaps by the overall lack of analysis of the failure mechanism when a material is utilized in an energy-storage device. In this study, we examined the reactivity of phenothiazine derivatives, which have found interest as redox shuttles in lithium-ion battery applications. We explored the products of the reactions of neutral compounds in battery electrolytes and the products of radical cation formation using bulk electrolysis and coin cell cycling. Following the failure of each cell, the electrolytes were characterized to identify redox shuttle decomposition products. Based on these results, a set of decomposition mechanisms is proposed and further explored using experimental and theoretical approaches. The results highlight the necessity to fully characterize and understand the chemical degradation mechanisms of the redox species in order to develop new generations of electroactive materials.

Introduction

The redox stability and reactivity of aromatic compounds are of immense interest across a broad landscape of electronic and energy storage applications. Singly oxidized (or reduced) aromatic molecules, for instance, are the active charge carriers in thin-film organic field-effect transistors,[1] solar cells,[2] and light-emitting diodes,[3] serve as redox shuttles in dye-sensitized solar cells[4] and in ion-intercalation batteries,[5] and act as catholytes (or anolytes) in redox flow batteries.[6] In each instance, the radical-cation (or radical-anion) forms of such compounds are sources of chemical decomposition and/or reactivity than can ultimately degrade device performance. Hence, it is essential to understand the stability and reactivity of these redox species to develop robust molecular systems that allow for enhanced device interrogation and performance.

Turning more specifically to electrochemical energy storage applications, the redox activity of aromatic molecules plays integral roles in terms of device perofrmance and safety. For instance, one issue that leads to overheating and degradation in lithium-ion batteries (LIBs) is overcharge, a condition that occurs when cell voltage rises beyond the maximum state of charge for the electrode couple, and can result in heat generation, electrolyte decomposition, and electrode damage. Redox shuttles are electrolyte additives that can improve the safety profiles of LIBs by protecting against overcharge.[7, 8] These additives limit battery voltage via redox processes that occur at each electrode / electrolyte interface when the oxidation potential of the redox shuttle is reached. A typical cycle of overcharge protection by redox shuttles involves (1) oxidation to the radical-cation state at the cathode / electrolyte interface, (2) diffusion to the anode, (3) regeneration of the neutral species at the anode / electrolyte interface via reduction, and (4) diffusion back to the cathode (Figure 1).

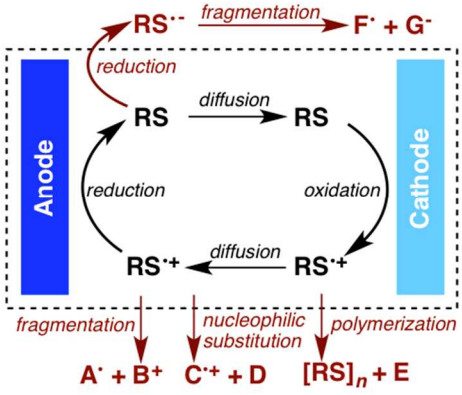

Figure 1. Mechanism of redox shuttle function during overcharge (black) and some possible decomposition pathways (red).

A limited number of molecular classes have been reported as redox shuttles with extensive overcharge protection capabilities. Many redox shuttles share a common electro-active redox core. The first examples of redox shuttles were metallocenes;[9, 10] since then, derivatives of TEMPO,[11] dimethoxybenzene,[12-18] triphenylamine,[19] and phenothiazine[20] have exhibited overcharge protection. Discovery of new redox shuttles has been achieved primarily by means of trial-and-error, with the redox cores further functionalized to modify oxidation potential, solubility, diffusion coefficient, or other physical properties. Although a number of unofficial rules have been developed regarding successful redox shuttle functionality and design, the number of long-lived redox shuttles thus far reported remains modest.

Outside of the normal redox cycle, the reactivity of redox shuttles in the battery environment remains largely unknown. Some of the numerous possible mechanisms by which redox shuttle molecules may be removed from circulation[21] are represented in Figure 1, including fragmentation, nucleophilic attack, and polymerization of the radical cation form. Alternately, the neutral redox shuttle may be reduced at the anode / electrolyte interface to form a radical anion, which could in turn decompose to yield a neutral radical and an anion. Many studies have reported the use of computational methods to calculate free energies of reaction for various decomposition pathways of redox shuttles[17, 18, 22] and other electrolyte additives[23, 24] as well as to investigate the stability of oxidized redox shuttles[5, 25-28] or the reversibility of electrochemical events.[29] However, analyses of redox shuttle byproducts have been largely limited to calculations. Chen and Amine analyzed the decomposition of 2,3,5,6-tetrafluoro-1,4-di-*tert*-butoxybenzene[30] and found that dealkylation occurred at high potentials, producing 2,3,5,6,-tetrafluoroquinone as a byproduct. Based on these results, the authors postulated that a similar mechanism might occur with the more commonly-studied derivative, 2,5-di-*tert*-butyl-1,4-dimethoxybenzene (DDB). With this possible exception, to the best of our knowledge, besides our own work,[31] no studies have been reported on the direct identification of redox shuttle decomposition products produced in LIB environments.

The fate of current-generation redox shuttles in LIBs has consequences for the design of new higher-potential or longer-lived analogues. Analysis of the electrolyte and electrode surfaces subsequent to coin cell failure is a logical next step in determining what reactions have occurred. We envision a systematic approach to studying redox shuttles and identifying the decomposition products produced in LIB environments. In particular, our research group is interested in phenothiazine-based redox shuttles (Figure 2). Although phenothiazines have lower oxidation potentials (*i.e.,* are easier to oxidize) than the more commonly studied dialkoxybenzene redox shuttles, they provide a generally robust aromatic core, and their oxidation potentials can be increased via the incorporation of electron-withdrawing substituents. A number of derivatives have been developed in recent years with substituents on the nitrogen atom as well as on the aromatic ring system, some of which are displayed in Table 1. Notably, variation in oxidation potentials and in overcharge performance is observed when these systems are studied in equivalent LIB environments. Here, we have assembled a group of diverse phenothiazine derivatives to allow us to elucidate decomposition mechanisms and to determine trends between structure and performance.

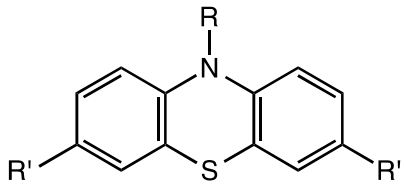

Figure 2. Representation of phenothiazine (R, R' = H) and derivatives under consideration, including variations in which R = H, alkyl, or aryl group and R' = H, Cl, Br, or CF_3.

Table 1. Substituted phenothiazine redox shuttles, half-wave oxidation potentials vs. $Li^{+/0}$ in 1.2 M $LiPF_6$ in EC/EMC (3:7 wt. ratio), and number of cycles of overcharge protection.

Redox Shuttle	R	R'	$E^{+/0}_{1/2}$ (V) vs. $Li^{+/0}$ [a]	Overcharge Cycles [b]
MPT	CH_3	H	3.55	3, 5 [c]
EPT	CH_2CH_3	H	3.51	127, 139 [c]
				20, 27, 65 [d]
iPrPT	$CH(CH_3)_2$	H	3.59	117, 118 [c]
tBuPT	$C(CH_3)_3$	H	3.45	2, 2 [c]
AcPT	$COCH_3$	H	4.08	0, 0
PhPT	C_6H_5	H	3.52	128, 161 [b]
DClEPT	CH_2CH_3	Cl	3.64	19, 22, 37 [c]
DBrEPT	CH_2CH_3	Br	3.66	2, 4, 5 [c]
BCF3EPT	CH_2CH_3	CF_3	3.83	17, 75, 242 [c, e]

[a] 1.2 M $LiPF_6$ in EC:EMC (3:7 wt. ratio); voltammograms recorded with a scan rate of 100 mV/s. [b] 100% overcharge at C/10 rate observed in synthetic graphite / $LiFePO_4$ coin cell batteries containing 0.08 M redox shuttle in 1.2 M $LiPF_6$ in EC:EMC (3:7 wt. ratio). [c] reference [31], [d] reference [26], [e] reference [28]

Experimental

Materials

Lithium iron phosphate ($LiFePO_4$) cathodes were purchased from Piotrek (Japan). The synthetic graphite anode, or 'Gen-2 anode,' (92 wt.% MAG-10 graphite (Hitachi), 8 wt.% polyvinylidene fluoride) was donated by Argonne National Laboratory (Argonne, IL). Trilayer polymer separator Celgard 2325 was donated by Celgard (Charlotte, USA). Ethylene carbonate (EC), ethyl methyl carbonate (DMC), and lithium hexafluorophosphate ($LiPF_6$) were purchased from BASF Corporation (NJ, USA). Tetra(*n*-butyl)ammonium hexafluorophosphate (electrochemical grade) and tris(4-bromophenyl)ammoniumyl hexachloroantimonate (technical grade) were purchased from Sigma-Aldrich. Anhydrous dichloromethane (DCM) and tetrahydrofuran (THF) were purchased from Fisher Scientific. PT and MPT were purchased from Sigma Aldrich. All other redox shuttles were synthesized as previously reported.[25-27, 31]

Tris(2,4-dibromophenyl)amine and tris(2,4-dibromophenyl)aminium hexachloroantimonate was synthesized following previously-reported procedures.[32] Silica gel (65 × 250 mesh) was purchased from Sorbent Technologies.

Electrochemical characterization

Redox shuttles were dissolved at 3 mM in 1.2 M $LiPF_6$ in ethylene carbonate / ethyl methyl carbonate (EC/EMC, 3:7 wt. ratio) in an argon-filled glove box. Cyclic voltammograms and differential pulse voltammograms were obtained using a CH Instruments 605E potentiostat with a three-electrode cell utilizing a 3 mm diameter glassy carbon working electrode, platinum wire counter electrode, and Li reference electrode. Voltammograms were obtained between 0 and 3 V versus $Li^{+/0}$ at 100 mV/s scan rates and in 10 mV increments, respectively.

Battery Fabrication, Cycling, and Analysis

Preparation of coin cells and cycling. Coin cells were assembled using synthetic graphite and $LiFePO_4$ electrodes containing 0.08 M redox shuttle in 1.2 M $LiPF_6$ in EC/EMC (3:7 wt. ratio) in an argon-filled glove box. Coin cells were charged at C/10 rate for 20 h (100% overcharge) followed by discharge at C/10 rate for 10 h. Cycling continued until cell voltage reached 5 V following redox shuttle failure.

Post-mortem battery breakdown and analysis. Subsequent to cycling experiments and redox shuttle failure, coin cells were disassembled and the internal battery components were extracted with ca. 5 mL of DCM. The organic extracts were filtered and concentrated under reduced pressure. The organic residue was subjected to analysis by electrospray ionization mass spectrometry (ESI-MS). Samples were dissolved in acetonitrile/water (2:1) prior to analysis. ESI mass spectra were obtained on a Thermo Finnigan LTQ ion trap mass spectrometer, with sample introduction by direct infusion via syringe pump at 3 μL/min. Full-scan mass spectra were recorded in positive-ion mode. Instrument parameters included spray voltage: 3.5 kV, capillary temperature: 185 ºC, capillary voltage: 50 V, and tube lens voltage: 80 V. Electrodes and separators were retained for further analysis.

SEM/EDX analysis of separators. SEM and EDX studies were carried out using a Hitachi S-4800 FE-SEM equipped with a transmitted electron detector and an Oxford EDS system, operated at 10 kV. Separators extracted from failed coin cells were fastened to the SEM holder using carbon tape. The samples were sputtered with gold for 30 s before SEM examination.

Chemical Oxidation and Reduction

Oxidation of Redox Shuttles with Bulk Electrolysis. Redox shuttles were oxidized by bulk electrolysis to observe their stability and reactivity over time under various conditions. MPT was dissolved at 0.1 M in DCM containing 0.1 M tetra*(n*-butyl)ammonium hexafluorophoshate with and without 1 M MeOH. Bulk electrolysis was conducted using a CH Instruments 605E potentiostat with a three-electrode setup utilizing a platinum coil as the working electrode, platinum wire as the counter electrode, and freshly anodized silver / silver chloride as the working electrode. Electrolysis of the solutions at 0.9 V vs. $Ag^{+/0}$ was performed for 5 min until a dark red color resulted. Samples were then maintained at room temperature to observe the stability of the characteristic radical-cation color over time.

Treatment of AcPT Radical Cation with a Chemical Oxidant. *N*-Acetylphenothiazine (0.30 g, 1.2 mmol) was dissolved in anhydrous DCM (5 mL) and purged with nitrogen. Tris(2,4-dibromophenyl)aminium hexachloroantimonate (0.13 g, 0.12 mmol) was added and the mixture was stirred for 15 min before being filtered. The resulting solid was washed with hexane and DCM and analyzed by X-ray crystallography.

Treatment of Redox Shuttles with a Chemical Reductant. Redox shuttles were treated with a reducing agent to probe the stability of neutral redox shuttles under reducing conditions. The redox shuttle (0.1 mmol) was dissolved in dry THF (1 mL), and the solution was purged with N_2 to deoxygenate. A solution of 1 M lithium naphthalenide (1 mL) was added to the redox shuttle solution in 10-fold excess, after which the reaction mixture was stirred for 1 h at room temperature. An aqueous saturated solution of ammonium chloride was then added to the reaction mixture, and the organic components were extracted with diethyl ether. The organic extracts were washed with brine, dried over anhydrous magnesium sulfate, and filtered to remove the drying agent. The organic residue was then analyzed by GC/MS and TLC to identify the isolated components. GC/MS spectra were obtained on an Agilent 5973N mass-selective detector attached to Agilent 6890N Network GC system.

DFT calculations

Density functional theory (DFT) calculations were performed using the Gaussian09 (Revision A.02b) software suite.[33] Geometry optimizations of the neutral, radical-cation, and radical-anion states were carried out with the B3LYP functional[34, 35] and 6-311G(d,p) basis set. Frequency analyses for each optimized geometry were undertaken to ensure that the geometries were energetic minima. The energy of each decomposition pathway was determined from the energies for each product/reactant computed at the same level of theory. All energies were refined using their respective zero-point energy corrections.

Results and Discussion

Post-Mortem Analysis of Cycled Batteries

Decomposition of the redox shuttle radical cation was suspected of leading to the inability of the electrolyte additives to prevent overcharge. In order to better understand the complex chemistry that occurs within the battery environment and to determine the fate of

redox shuttles, we first sought to determine what products form in LIBs during redox shuttle failure. Failed LIBs were opened, and the electrolyte was extracted using organic solvent to recover any remaining redox shuttles, fragmentation products, and other byproducts. These extracts were subjected to ESI-MS analysis to identify molecular ions present due to the redox shuttle decomposition. The analyses surveyed a wide *m/z* scan to observe fragments, adducts, and polymerized byproducts.

ESI is the ideal mass spectrometry technique for our study because it is a soft ionization method that does not typically cause fragmentation of molecular ions. Although ESI-MS typically produces adducts with protons or other cations, phenothiazine derivatives – due to their ease of oxidation – can be observed in their radical-cation states, albeit often accompanied by the corresponding adduct with an additional proton/cation. The mass spectra of the *N*-alkyl phenothiazine series are shown in Figure 3. The first spectrum contained in Figure 3 depicts the contents of a coin cell without a redox shuttle; this cell was analyzed to identify background peaks that originate from the battery components themselves (e.g. polymer fragments leached from the electrode binder or solid-electrolyte interface). The peaks observed in coin cells without redox shuttle are denoted with a red X when they appear in other spectra. A common decomposition product across the *N*-alkyl phenothiazine coin cells was *m/z* 199, which likely corresponds to unsubstituted phenothiazine (PT). Other common peaks were identified at *m/z* 395, 592, and 789. EPT and iPrPT spectra show peaks that correspond to their sulfoxide forms, with *m/z* 244 and 248, respectively.

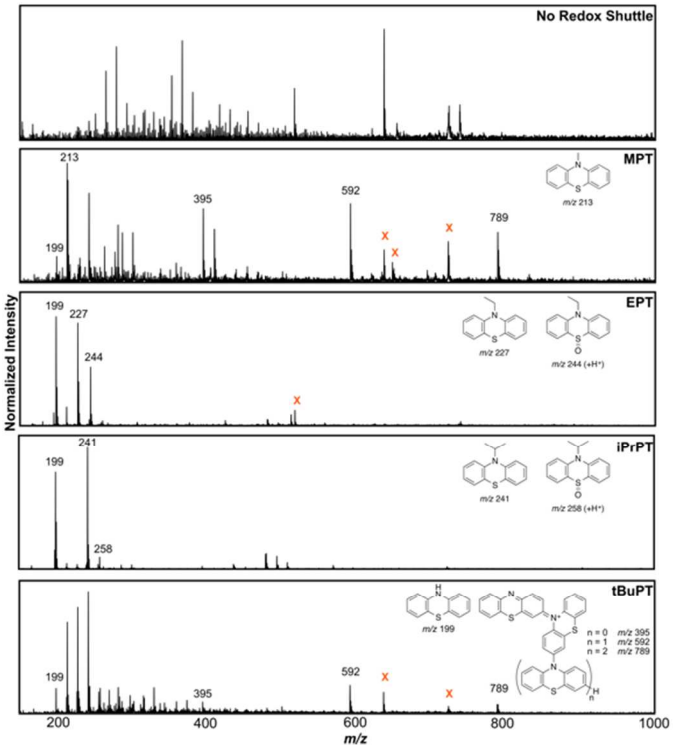

Figure 3. Post-mortem ESI analysis of contents extracted from cycled coin cells containing *N*-alkyl PT derivatives. Peaks of interest are labelled with *m/z* value. Peaks due to battery components are marked with red X.

A coin cell was assembled with phenothiazine, which has previously been reported to oxidatively couple,[36, 37] as the additive in order to determine whether larger oligomers form as the result of unsubstituted PT produced in the battery from the *N*-alkyl phenothiazines. The battery was cycled and analyzed following the same procedure as the other batteries. ESI-MS spectra of its contents (Figure 4) revealed peaks at *m/z* 395, 592 and 789, likely corresponding to oligomers of PT.

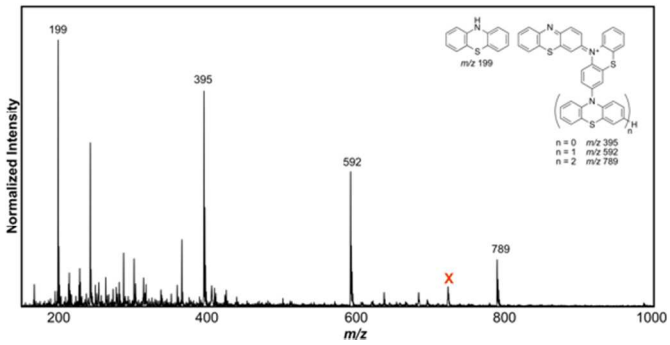

Figure 4. Post-mortem ESI analysis of contents extracted from a coin cell containing unsubstituted PT and proposed structures for some annotated peaks. Peaks of interest are labelled with *m/z* value. Peaks due to battery components are marked with a red X.

Our initial ESI-MS analyses suggest that redox shuttle decomposition occurs via various mechanisms and at different rates according to the identity of the shuttle. The substituent at the PT nitrogen atom is susceptible to reaction depending on the hybridization and substitution of the carbon atom directly connected to nitrogen.[31] Amongst the alkyl-substituted derivatives, MPT and tBuPT exhibit significant amounts of decomposition and polymerization in ESI-MS analysis, while EPT and iPrPT show relatively little decomposition product formation. These observations correlate with cell-cycling experiments in which EPT and iPrPT outperform MPT and tBuPT in protecting against overcharge. Fragmentation of these radical cations is energetically favorable,[31] but the rate of each reaction depends on its transition state barrier. No common mechanism for alkyl-substituted PTs can be identified (Scheme 1), as both S_N1 and S_N2 reactions are likely to occur depending on structure of the substituent. Fundamental principles of substitution reactions suggest that dealkylation of MPT follows an S_N2-like mechanism and dealkylation of tBuPT follows an S_N1-like mechanism. EPT and iPrPT are less prone to dealkylate via an S_N2 mechanism thanks to additional substitution at the position alpha to the nitrogen, nor are ethyl or isopropyl cations stable enough to suggest dealkylation via an S_N1 mechanism.

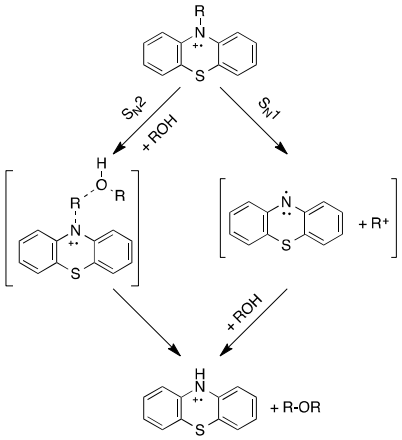

Scheme 1. *N*-Alkyl fragmentation via S_N1 and S_N2 mechanisms.

Although AcPT has been reported as an effective redox shuttle,[20] we have been unable to successfully employ it as a stable redox shuttle in coin cells. In contrast, PhPT showed extensive overcharge protection abilities in batteries cycled under the same conditions. Not surprisingly, the mass spectra of coin cell components containing AcPT differed significantly from the more robust PhPT variant despite both having sp^2-hybridized substituents. ESI-MS of AcPT (Figure 5) shows essentially complete decomposition to form PT (m/z 199) with very few oligomers present. In the case of PhPT (Figure 4), formation of PT was not observed. Prominent peaks included *m/z* 275 and 292, which can be attributed to PhPT and PhPT sulfoxide (proton adduct), respectively.

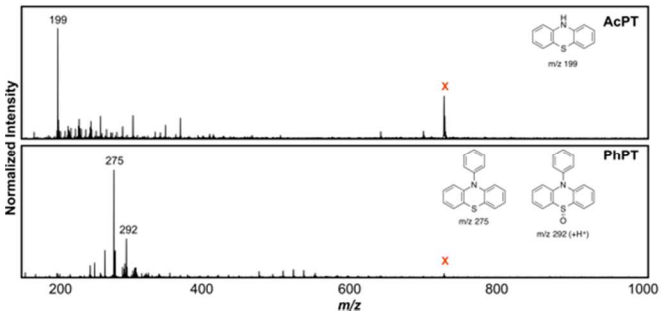

Figure 5. Post-mortem ESI-MS of contents extracted from coin cells containing AcPT and PhPT. Peaks of interest are labelled with *m/z* value. Peaks due to battery components are marked with red X.

It is likely that AcPT decomposes upon cell cycling to form the PT radical cation, which may further oligomerize (Scheme 2). The formation of the stable acylium cation may be a driving force for decomposition upon oxidation in the coin cell. This further emphasizes the importance of a stable substituent at the PT nitrogen, particularly one that cannot form a stabilized cation. We treated AcPT with the oxidant tris-(2,4-dibromophenyl)aminium hexachloroantimonate in dichloromethane (DCM) and observed the formation of a PT dimer, as identified by X-ray crystallographic analysis.† By contrast, cleavage of the phenyl substituent from PhPT would result in a highly unstable phenyl cation. This high-energy fragment likely makes the fragmentation reaction barrier prohibitively high for decomposition via this pathway. PhPT, as well as the long-lived redox shuttles EPT and iPrPT, demonstrate limited fragmentation (although they do oxidize to the sulfoxide form, which does not function as an effective redox shuttle).

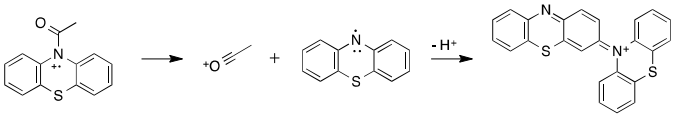

Scheme 2. Proposed mechanism for the decomposition of AcPT into PT dimer.

Although EPT showed simple, if limited, fragmentation of the *N*-ethyl group, substituted EPTs exhibited variable reactivity patterns in coin cells. DClEPT (Figure 6) exhibited peaks primarily at *m/z* 295/297/299 (intact DClEPT) and 266/268/270 (loss of the ethyl group). No noticeable oligomers formed, which is likely due to the chlorine atoms at the 3- and 7-positions preventing reaction at the usually reactive *para* position. Interestingly, the spectrum of DBrEPT (Figure 5) showed no trace of DBrEPT, nor were there characteristic isotope patterns for fragments containing bromine. Peaks at *m/z* 199 and 227 were observed, which correspond to PT and EPT respectively. These peaks suggest the facile reduction of the C–Br bond in the battery environment. BCF3EPT (Figure 5) exhibited peaks at *m/z* 335 and 363, corresponding to *N*-dealkylated and original BCF3EPT, respectively. A peak at *m/z* 380 is also present, which suggests the formation of BCF3EPT sulfoxide.

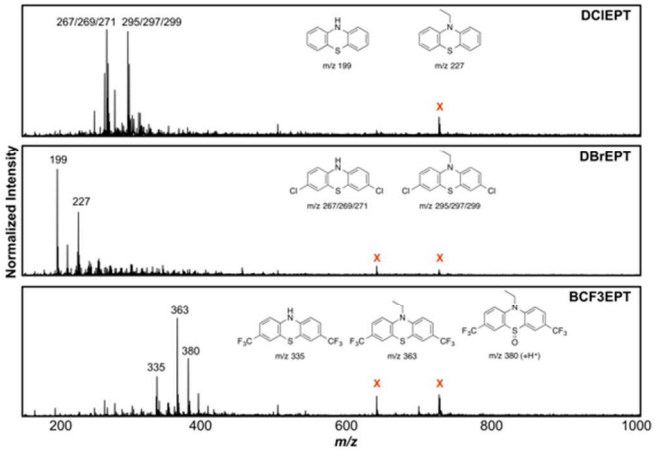

Figure 6. Post-mortem ESI-MS of coin cells containing DClEPT, DBrEPT, or BCF3EPT. Peaks of interest are labelled with *m/z* value. Peaks due to battery components are marked with a red X.

A notable observation from the evaluation of disassembled battery components was the discoloration of the separator in the coin cell containing DBrEPT. In other batteries, we did not observe discoloration of polymer separators after cycling, but the separator from the coin cell containing DBrEPT was deep orange in color (Figure 7a-b). In an attempt to identify the cause of this color change, we compared separators from coin cells with no redox shuttle, coin cells containing EPT, and coin cells containing DBrEPT using SEM with EDX analysis (Figure 7e-f). We saw no noticeable

differences in morphology among SEM images collected of the separators. EDX analysis showed no incorporation of sulfur or nitrogen into the separator, as would be expected if the redox shuttle reacted with or was deposited onto the separator surface. However, in the case of DBrEPT, we observed signals in the separator that correspond to bromine and copper. The incorporation of bromine into the separator further supports the reduction of DBrEPT in the coin cell. The reduction of DBrEPT could produce bromide ions upon fragmentation of the C-Br bonds in the DBrEPT radical anion, which could then be oxidized to molecular bromine at the cathode. Molecular bromine (Br_2) could then react with metallic current collectors, which may explain the presence of copper in the separator.

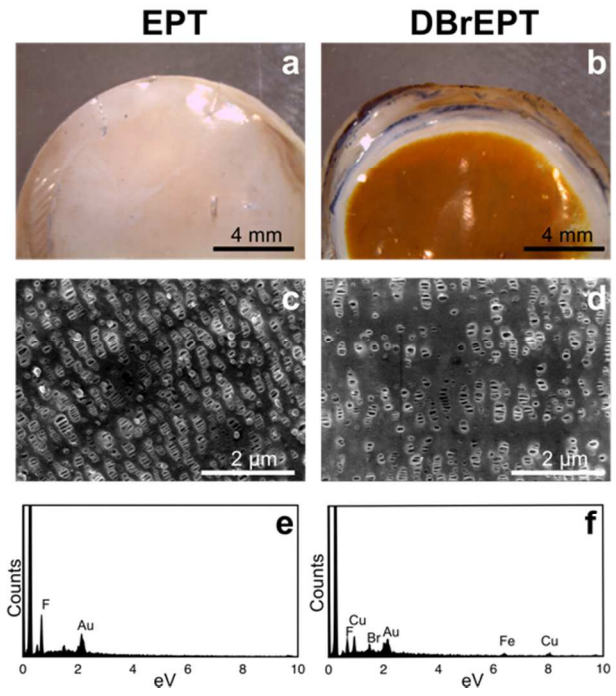

Figure 7. Micrograph of separator from coin cells containing EPT (a) or DBrEPT (b). SEM of separator containing EPT (c) or DBrEPT (d). EDX spectra of separator from coin cells containing EPT (e) or DBrEPT (f).

Analyzing the Stability and Reactivity of Redox Shuttles

To gain further insight into the nature of the decomposition mechanisms, we examined the nucleophilic decomposition of *N*-substituted phenothiazine radical cations via reaction with methanol (MeOH), which serves as a model oxygen-centered nucleophile, as depicted in Scheme 3. Energies for each reactant and product were determined from DFT geometry optimizations at the B3LYP/6-311G(d,p) level of theory and then used to calculate energies of reaction. In all cases, the reactions are exothermic (Table 2). Although this suggests that *N*-substituted phenothiazine fragmentation is energetically favourable, it does not imply that all derivatives will fragment readily in batteries. Rather, each transition state and its associated energetic barrier (*i.e.,* reaction kinetics) will likely determine the extent of decomposition in the battery: Some dealkylation mechanism transition barriers may be too high for dealkylation to take place rapidly or in appreciable amounts.

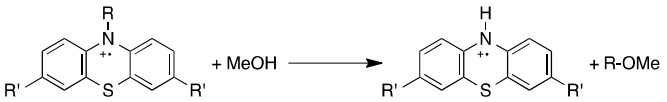

Scheme 3. Reaction of the radical cation of a generic phenothiazine derivative with methanol to form the dealkylated radical cation.

Table 2. Reaction energies (ΔE_{rxn}) for each radical cation fragmentation with MeOH as the nucleophile as obtained at the B3LYP/6-311G(d,p) level of theory.

Redox Shuttle	ΔE_{rxn} (kcal/mol)
MPT	- 2.45
EPT	- 6.53
iPrPT	- 9.98
tBuPT	- 17.83
AcPT	- 26.76
PhPT	- 3.62
DClEPT	- 6.02
DBrEPT	- 6.15
BCF3EPT	- 4.09

To confirm that MeOH is a valid approximation for the redox shuttle decomposition reaction, we subjected some redox shuttles to bulk electrolysis in the presence and absence of MeOH. Bulk electrolysis was conducted using 100 mM solutions of MPT in DCM containing 100 mM tetra(*n*-butyl)ammonium hexafluorophosphate. In the absence of MeOH, MPT radical cation shows no decay into PT. However, in the presence of 1 M MeOH, the characteristic red color of MPT radical cation adopts a bluish color overnight, which suggests decomposition and oligomerization.

The choice of substituent at the nitrogen position also affects performance, as can be seen from the series of *N*-substituted phenothiazines. Derivatives containing the largest (tBuPT) and smallest (MPT) substituents suffered from being the most reactive in S_N1 and S_N2 reactions, respectively. By contrast, primary and secondary carbon atoms in EPT and iPrPT render them less reactive via both mechanisms, leading to more stable radical cations. We further suspect that PhPT demonstrates extended overcharge protection abilities because the substituent at the *N*-position contains a sp^2-hybridized carbon atom, which cannot react in S_N1 or S_N2 reactions. Substituents at the *N*-position that allow for facile cleavage of the C-N bond are also detrimental to redox shuttle performance, as was the case with AcPT.

Although the stability of *N*-substituted phenothiazines tends to be associated with the reactivity of the oxidized state, *N*-ethyl phenothiazines containing substituents on the aromatic core follow different patterns of reactivity. Because it appears that DBrEPT

forms de-brominated EPT and de-brominated, dealkylated PT during battery cycling, we suspect that stability under reducing conditions might play a role in redox shuttle stability. With this in mind, we treated the substituted EPTs with a chemical reducing agent, lithium naphthalenide, which is similar in reducing power to the lithiated (charged) graphitic anode (Scheme 4). EPT itself was unreactive toward the reducing agent, with no decomposition to byproducts observed by GC/MS or TLC. DBrEPT and DClEPT were both reduced to EPT upon treatment with lithium naphthalenide; BCF3EPT exhibited diminished reactivity as well as decomposition to unknown products (as analyzed via TLC).

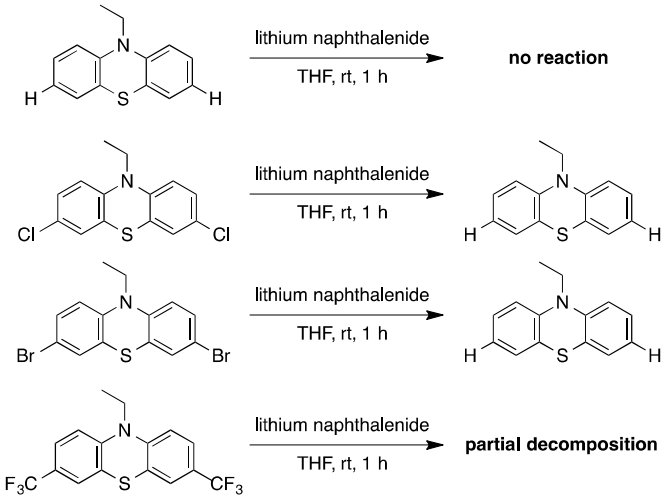

Scheme 4. Reaction of substituted EPT and disubstituted derivatives with the reducing agent lithium naphthalenide.

We recorded the voltammograms of EPT and its substituted derivatives via cyclic voltammetry (CV) and differential pulse voltammetry (DPV) to determine whether any reduction events occur at low potentials. Voltammograms from CV experiments (Figures S1-S5) were difficult to interpret because reduction peaks are close to the solvent window. DPV was more useful, showing an irreversible reduction for both DBrEPT and DClEPT at ca. 0.5 V and 0.4 V vs. $Li^{+/0}$, respectively (Figure 8). Although we do not observe decomposition products from DClEPT reduction in coin cells, we do find reduction products of DBrEPT, consistent with its higher reduction potential (*i.e.,* easier to reduce) obtained from the DPV experiments. The stability of the redox shuttle at a wide range of potentials in the battery environment is indeed important for determining redox shuttle stability.

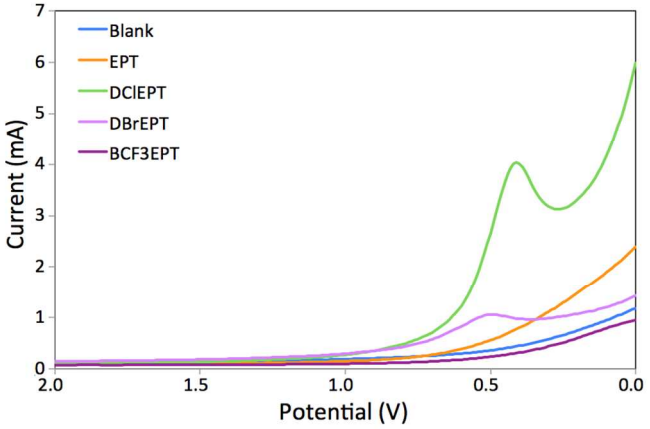

Figure 8. Voltammograms from DPV experiments of EPT and disubstituted EPT derivatives showing a reduction at 0.52 V vs. $Li^{+/0}$ for DBrEPT and a reduction at 0.42 V vs. $Li^{+/0}$ for DClEPT.

DFT calculations were once again employed in an attempt to understand decomposition pathways, this time targeting decomposition reactions that might result from redox shuttle reduction in battery environments. Electron affinities for the substituted EPT series and energies for possible radical anion decomposition pathways (Scheme 5) are given in Table 3. As electron-withdrawing groups are added to the EPT core, the electron affinity increases (as expected). DBrEPT and BCF3EPT both exhibit high electron affinities, suggesting that these compounds might act as electron acceptors in the battery environment. DClEPT exhibits a limited electron affinity, meaning it is less likely to accept an electron, which may explain why C–Cl bond reduction is not observed in coin cells. The fragmentation energy for the removal of R' (R' = Br^-, Cl^-, CF_3^-) reveals that the Cl and Br substituents undergo more ready cleavage than CF_3 or H. Combined with the reduction energies, these results suggest that DBrEPT should be most prone to decomposition, which agrees with the battery cycling experiments.

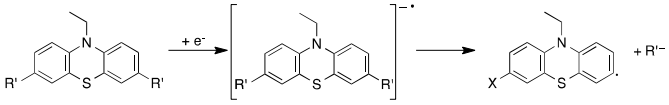

Scheme 5. Mechanism of cleavage of C-X bonds upon reduction of disubstituted EPT derivatives.

Table 3. Energies for reduction and for fragmentation of the subsequently formed radical anion as obtained at the B3LYP/6-311G(d,p) level of theory.

Redox Shuttle	$\Delta E_{reduction}$ [a] (kcal/mol)	$\Delta E_{fragmenation}$ (kcal/mol)
EPT	+ 12.85	+ 92.28
DClEPT	- 0.37	+ 4.87
DBrEPT	- 12.61	+ 13.42
BCF3EPT	- 9.76	+ 85.76

[a] $\Delta E_{reduction} = E_{anion} - E_{neutral}$; hence, a negative $\Delta E_{reduction}$ indicates an energetically stable radical anion.

Conclusions

Substituted phenothiazine derivatives offer the opportunity to tune redox shuttle operating potentials as well as stability and other physical properties. From this study, it becomes readily apparent that care must be taken during the molecular design stage, as modest differences in the substituents on the aromatic core can have profound affects. The introduction of halogens increases the operating potential of redox shuttles, which is desirable for overcharge protection in high voltage LIBs. However, the electron-withdrawing groups also raise reduction potentials, making reduction at the (lithiated) graphitic carbon anode easier, as was the case with DBrEPT, which contains weaker bonds than its more robust counterparts, DClEPT and BCF3EPT.

This study on the byproducts of PT-based redox shuttles allows us a better understanding of the reactivity of the PT core and substituent effects on redox shuttles. It is apparent that the stability of side-chains on the heteroatom is of the utmost importance when designing new PT-based redox shuttles, specifically to avoid reactivity through S_N1 and S_N2 pathways. Ethyl, isopropyl and phenyl derivatives offer the best balance of stability under both reaction pathways. The trifluoromethyl group appears to be a highly stable functional group that is capable of increasing the operating redox shuttle potential while simultaneously stabilizing the radical cation form, thereby increasing effective lifetime.

Even long-lived redox shuttles ultimately fail when the concentration of active material decreases below the concentration at which it is able to shuttle electrons for a given charge rate. It appears that for EPT, iPrPT, PhPT and BCF3EPT that reduced effectiveness arises from the gradual oxidation to their respective sulfoxide forms. It may be possible to design other substituents that offer the same stability as well as enable tuning of oxidation potentials or physical properties for enhanced redox shuttle performance. Tuning of the redox core with substituents is an important tool for tailoring redox shuttles to different electrode systems, but careful consideration of functional groups is key.

Acknowledgements

We thank the American Chemical Society Petroleum Research Fund for partial support of this research through a Doctoral New Investigator Award, as well as the National Science Foundation, Division of Chemistry for Award Number CHE-1300653. SAO and CR thank the University of Kentucky Vice President for Research for start-up funds and the High Performance Computing Facility for supercomputer access. We thank Jack Goodman at the University of Kentucky Mass Spectrometry facility for his assistance obtaining mass spectrometry data. We also thank Andrew Jansen and Bryant Polzin at the Cell Manufacturing and Modelling Center at Argonne National Laboratory for battery electrode materials and helpful discussions. Lastly we thank Dr. Sean Parkin at the University of Kentucky X-ray Crystallography Facility for analysis of solid products.

Notes and references

[a] Department of Chemistry, University of Kentucky, Lexington, KY, USA, 40506.
[b] Center for Applied Energy Research, University of Kentucky, Lexington, KY, USA, 40511.
Corresponding author e-mails: chad.risko@uky.edu, susan.odom@uky.edu

† The exact structure of the dimer could not be determined due to the poor quality of the crystals. It is clear that the structure is a dimer, but multiple possibilities were possible for the substituents.

Electronic Supplementary Information (ESI) available: cyclic voltammograms. See DOI: 10.1039/b000000x/

1. H. Sirringhaus, P. J. Brown, R. H. Friend, M. M. Nielsen, K. Bechgaard, B. M. W. Langeveld-Voss, A. J. H. Spiering, R. A. J. Janssen, E. W. Meijer, P. Herwig and D. M. de Leeuw, *Nature*, 1999, **401**, 685-688.
2. C. J. Brabec, N. S. Sariciftci and J. C. Hummelen, *Adv. Fun. Mater.*, 2001, **11**, 15-26.
3. C. D. Muller, A. Falcou, N. Reckefuss, M. Rojahn, V. Wiederhirn, P. Rudati, H. Frohne, O. Nuyken, H. Becker and K. Meerholz, *Nature*, 2003, **421**, 829-833.
4. T. W. Hamann and J. W. Ondersma, *Energy & Environmental Science*, 2011, **4**, 370-381.
5. L. M. Moshurchak, C. Buhrmester and J. R. Dahn, *J. Electrochem. Soc.*, 2005, **152**, A1279-A1282.
6. F. R. Brushett, J. T. Vaughey and A. N. Jansen, *Advanced Energy Materials*, 2012, **2**, 1390-1396.
7. L. M. Moshurchak, C. Buhrmester, R. L. Wang and J. R. Dahn, *Electrochim. Acta*, 2007, **52**, 3779-3784.
8. Z. Chen, Y. Qin and K. Amine, *Electrochim. Acta*, 2009, **54**, 5605-5613.
9. M. N. Golovin, D. P. Wilkinson, J. T. Dudley, D. Holonko and S. Woo, *J. Electrochem. Soc.*, 1992, **139**, 5-10.
10. K. M. Abraham, D. M. Pasquariello and E. B. Willstaedt, *J. Electrochem. Soc.*, 1990, **137**, 1856-1857.
11. C. Buhrmester, L. M. Moshurchak, R. L. Wang and J. R. Dahn, *J. Electrochem. Soc.*, 2006, **153**, A1800-A1804.
12. J. Chen, C. Buhrmester and J. R. Dahn, *Electrochem. Solid-State Lett.*, 2005, **8**, A59-A62.
13. J. R. Dahn, J. Jiang, L. M. Moshurchak, M. D. Fleischauer, C. Buhrmester and L. J. Krause, *J. Electrochem. Soc.*, 2005, **152**, A1283-A1289.
14. Z. Chen and K. Amine, *Electrochem. Commun.*, 2007, **9**, 703-707.
15. J. K. Feng, X. P. Ai, Y. L. Cao and H. X. Yang, *Electrochem. Commun.*, 2007, **9**, 25-30.
16. L. M. Moshurchak, W. M. Lamanna, M. Bulinski, R. L. Wang, R. R. Garsuch, J. Jiang, D. Magnuson, M. Triemert and J. R. Dahn, *J. Electrochem. Soc.*, 2009, **156**, A309-A312.
17. W. Weng, Z. Zhang, P. C. Redfern, L. A. Curtiss and K. Amine, *J. Power Sources*, 2011, **196**, 1530-1536.
18. L. Zhang, Z. Zhang, P. C. Redfern, L. A. Curtiss and K. Amine, *Energy Environ. Sci.*, 2012, **5**, 8204-8207.
19. L. M. Moshurchak, C. Buhrmester and J. R. Dahn, *J. Electrochem. Soc.*, 2008, **155**, A129-A131.
20. C. Buhrmester, L. Moshurchak, R. L. Wang and J. R. Dahn, *J. Electrochem. Soc.*, 2006, **153**, A288-A294.
21. M. Schmittel and A. Burghart, *Angew. Chem. Int. Ed.*, 1997, **36**, 2550-2589.
22. Z. Zhang, L. Zhang, J. A. Schlueter, P. C. Redfern, L. Curtiss and K. Amine, *J. Power Sources*, 2010, **195**, 4957-4962.

23. O. Borodin, W. Behl and T. R. Jow, *J. Phys. Chem. C*, 2013, **117**, 8661-8682.
24. S. Kaymaksiz, F. Wilhelm, M. Wachtler, M. Wohlfahrt-Mehrens, C. Hartnig, I. Tschernych and U. Wietelmann, *J. Power Sources*, 2013, **239**, 659-669.
25. S. A. Odom, S. Ergun, P. P. Poudel and S. R. Parkin, *Energy Environ. Sci.*, 2014, **7**, 760-767.
26. S. Ergun, C. F. Elliott, A. P. Kaur, S. R. Parkin and S. A. Odom, *Chem. Commun.*, 2014, **50**, 5339-5341.
27. S. Ergun, C. F. Elliott, A. P. Kaur, S. R. Parkin and S. A. Odom, *J. Phys. Chem. C*, 2014, **118**, 14824-14832.
28. A. P. Kaur, S. Ergun, C. F. Elliott and S. A. Odom, *J. Mat. Chem. A*, 2014, **2**, 18190-18193.
29. S. Kaymaksiz, M. Wachtler and M. Wohlfahrt-Mehrens, *J. Power Sources*, 2015, **273**, 123-127.
30. Z. Chen and K. Amine, *Electrochimica Acta*, 2007, **53**, 453-458.
31. K. A. Narayana, M. D. Casselman, C. F. Elliott, S. Ergun, S. R. Parkin, C. Risko and S. A. Odom, *ChemPhysChem*, manuscript accepted for publication.
32. W. Schmidt and E. Steckhan, *Chem. Ber.*, 1980, **113**, 577-585.
33. G. W. T. M. J. Frisch, H. B. Schlegel, G. E. Scuseria, M. A. Robb, J. R. Cheeseman, G. Scalmani, V. Barone, B. Mennucci, G. A. Petersson, H. Nakatsuji, M. Caricato, X. Li, H. P. Hratchian, A. F. Izmaylov, J. Bloino, G. Zheng, J. L. Sonnenberg, M. Hada, M. Ehara, K. Toyota, R. Fukuda, J. Hasegawa, M. Ishida, T. Nakajima, Y. Honda, O. Kitao, H. Nakai, T. Vreven, J. A. Montgomery Jr., J. E. Peralta, F. Ogliaro, M. J. Bearpark, J. Heyd, E. N. Brothers, K. N. Kudin, V. N. Staroverov, R. Kobayashi, J. Normand, K. Raghavachari, A. P. Rendell, J. C. Burant, S. S. Iyengar, J. Tomasi, M. Cossi, N. Rega, N. J. Millam, M. Klene, J. E. Knox, J. B. Cross, V. Bakken, C. Adamo, J. Jaramillo, R. Gomperts, R. E. Stratmann, O. Yazyev, A. J. Austin, R. Cammi, C. Pomelli, J. W. Ochterski, R. L. Martin, K. Morokuma, V. G. Zakrzewski, G. A. Voth, P. Salvador, J. J. Dannenberg, S. Dapprich, A. D. Daniels, Ö. Farkas, J. B. Foresman, J. V. Ortiz, J. Cioslowski, D. J. Fox, 2009, Gaussian, Inc., Wallingford, CT, USA.
34. A. D. Becke, *J. Chem. Phys.*, 1993, **98**, 5648-5652.
35. C. Lang, W. Yang and R. G. Parr, *Phys. Rev. B*, 1988, **37**, 785-789.
36. P. Hanson and R. O. C. Norman, *J. Chem. Soc. Perkin Trans. 2*, 1973, 264-271.
37. L. G. Shagun, I. A. Dorofeev, I. A. Tokareva, V. I. Smirnov, V. A. Shagun and M. G. Voronkov, *Russ. J. Org. Chem.*, 2012, **48**, 1263-1264.

The Fate of Phenothiazine-Based Redox Shuttles in Lithium-Ion Batteries

Matthew D. Casselman, Aman Preet Kaur, Kishore Anand Narayana, Corrine F. Elliott, Chad Risko,* and Susan A. Odom*

Table of Contents Image: